Published on 05 August 2015. Downloaded by UNIVERSIDAD ESTADUAL DE CAMPINAS on 05/05/2016 19:33:05.

Dalton Transactions

PAPER

View Article Online
View Journal | View Issue

Cite this: *Dalton Trans.*, 2015, **44**, 15843

Controlling dimensionality *via* a dual ligand strategy in Ln-thiophene-2,5-dicarboxylic acid-terpyridine coordination polymers†

Korey P. Carter,[a] Cecília H. F. Zulato,[a,b] Emille M. Rodrigues,[b] Simon J. A. Pope,[c] Fernando A. Sigoli*[b] and Christopher L. Cahill*[a]

Received 8th July 2015,
Accepted 30th July 2015

DOI: 10.1039/c5dt02596f

www.rsc.org/dalton

Eleven new lanthanide (Ln = Nd-Lu)-thiophene-2,5-dicarboxylic acid (25-TDC)-2,2′:6′,2″-terpyridine (terpy) coordination polymers (**1–11**) which employ a dual ligand strategy have been synthesized hydrothermally and structurally characterized by single crystal and powder X-ray diffraction. Two additional members of the series (**12** and **13**) were made with Ce^{3+} and Pr^{3+} and characterized *via* powder X-ray diffraction only. The series is comprised of three similar structures wherein differences due to the lanthanide contraction manifest in Ln^{3+} coordination number as well as the number of bound and solvent water molecules within the crystal lattice. Structure type I (Ce^{3+}–Sm^{3+}) contains two nine-coordinate Ln^{3+} metal centers each with a bound water molecule. Structure type II (Eu^{3+}–Ho^{3+}) features a nine and an eight coordinate Ln^{3+} metal along with one bound and one solvent water molecule. Structure type III (Er^{3+}–Lu^{3+}) includes two eight-coordinate Ln^{3+} metal centers with both water molecules residing in the lattice. Assembly into supramolecular 3D networks *via* π–π interactions is observed for all three structure types, whereas structure types II and III also feature hydrogen-bonding interactions *via* the well-known C–H···O and O–H···O synthons. Visible and near-IR luminescence studies were performed on compounds **1**, **2**, **10**, and **13** at room temperature. As a result characteristic near-IR luminescent bands of Pr^{3+}, Nd^{3+}, Sm^{3+}, and Yb^{3+} as well as visible bands of Sm^{3+} were observed.

Introduction

The study of lanthanide hybrid materials incorporating conjugated carboxylic acids has garnered significant interest over the past decade due to their rich structural diversity and wide array of topologies. Crystalline hybrid materials are an area of structural chemistry that include coordination polymers (CPs) and metal–organic frameworks (MOFs), which can both be defined as assemblies of Ln^{3+} metal centers polymerized through organic linkers resulting in diverse topologies of higher dimensionality.[1,2] As such, these materials have proven particularly attractive for applications including luminescence,[3–5] sensing (cation, anion, or molecular),[6–8] gas storage,[9–11] heterogeneous catalysis,[12–15] and magnetism.[16–18]

Whereas CPs and MOFs with d-block metal compositions have been studied and reviewed extensively,[19–23] perhaps due to a propensity for formation of true MOFs and therefore gas storage/separation and catalytic applications, lanthanide hybrids represent a still-developing field which may be attributed to the unique nature of bonding in lanthanide materials. Inspired by the early works of Férey,[24] Yaghi,[3,25,26] and Chen[27] and the more recent efforts of Allendorf,[28,29] Almeida Paz[30] and Müller-Buschbaum[31,32] we endeavored to synthesize a series of lanthanide coordination polymers that provide a forum for further study of Ln^{3+} CP luminescence, while also presenting a platform allowing for exploration of supramolecular assembly.

Lanthanide luminescence remains a topic of great interest due to the unique, line-like nature of Ln^{3+} emission. Direct excitation of lanthanide metal centers is hindered by low molar absorption coefficients, small absorption cross-sections and the formally forbidden nature of f–f transitions,[33] thus Ln^{3+} emission often relies on the well-known antenna effect as

[a]*Department of Chemistry, The George Washington University, 800 22nd Street, NW, Washington, D.C. 20052, USA. E-mail: cahill@gwu.edu; Tel: +1 (202)994-6959*
[b]*Laboratory of Functional Materials, Institute of Chemistry, University of Campinas, UNICAMP, P. O. Box 6154, Campinas, Sao Paulo 13083-970, Brazil. E-mail: fsigoli@iqm.unicamp.br*
[c]*School of Chemistry, Main Building, Cardiff University, Cymru/Wales, CF10 3AT, UK*

†Electronic supplementary information (ESI) available: Additional single crystal XRD data, ORTEP figures of all compounds, PXRD spectra of all compounds, tables of selected bond lengths and supramolecular interaction distances, and X-ray crystallographic files in CIF. CCDC 1410403–1410413. For ESI and crystallographic data in CIF or other electronic format see DOI: 10.1039/c5dt02596f

Published on 05 August 2015. Downloaded by UNIVERSIDAD ESTADUAL DE CAMPINAS on 05/05/2016 19:33:05.

a means of absorbing incoming radiation and the subsequent sensitization of the Ln^{3+} metal center.[34] First reported in 1942, the antenna effect utilizes a ligand that does not suffer from parity forbidden transitions to absorb incoming light before transferring it to the excited states of the Ln^{3+} ion.[35,36] Efficient utilization of the antenna effect requires the selection of organic chromophores with triplet state energies in the appropriate range for sensitization (singlet states energies are often too high for Ln^{3+} sensitization), and our ligand selections were made explicitly with these criteria in mind.

Thiophene-2,5-dicarboxylic acid (2,5-TDC) is a heterofunctional organic linker with a triplet state in an appropriate range for Ln^{3+} sensitization (*ca.* 25 800 cm^{-1}) and has been used in a wide array of lanthanide coordination polymers over the past decade. First incorporated in a lanthanide hybrid material by Yaghi and colleagues in MOF-75,[37] 2,5-TDC has remained a organic linker of interest in lanthanide hybrids due to the interesting luminescent[38–42] and magnetic properties[43,44] displayed by these materials. Structurally, all 54 Ln-2,5-TDC materials in the CSD (v. 5.36, Nov. 2014)[45] are three dimensional coordination polymers, and approximately one-third (17/54) of these materials feature some Ln^{3+} oligomerization (dimers, chains, *etc.*).[43,46–48] Inspired by the dual ligand strategy we have explored previously with molecular lanthanide complexes as a means to control nuclearity at Ln^{3+} sites,[49,50] we herein endeavored to exercise some control over framework dimensionality by interrupting the connectivity of Ln-2,5-TDC networks *via* the addition of a capping ligand, in this case the tridentate 2,2′:6′,2″-terpyridine.

The addition of a co-(capping) ligand to 2,5-TDC hybrid materials has precedent within transition metal hybrids,[51–54] and is a concept explored in other lanthanide hybrids where researchers were looking to control interpenetration and enhance gas sorption properties.[55] Our efforts parallel the earlier contribution of Zhou *et al.*[55] as our choice of capping ligand was made with crystal engineering design principles explicitly in mind. We have been successful in controlling nuclearity with terpy in both molecular lanthanide[49] and uranyl materials,[56,57] and thus we selected terpy herein with the goal of extending this concept up to the topological level to influence the dimensionality of CPs built from a ditopic carboxylate and a capping ligand. Additionally, terpy has been shown to efficiently sensitize lanthanide emission[49,58,59] and represents an 'upgrade' as compared to 2,5-TDC (*i.e.* a lower T_1 energy value closer to the excited states of Ln^{3+} cations) when considering the guidelines outlined by Latva and colleagues.[60]

Herein we report the synthesis, crystal structures, supramolecular interactions and visible and near-IR luminescent properties (for the Pr^{3+}, Nd^{3+}, Sm^{3+} and Yb^{3+} members of the series) of a family of thirteen coordination polymers containing the organic ligands thiophene-2,5-dicarboxylic acid and 2,2′:6′,2″-terpyridine. Moreover, the consistent nature of both Ln–O and Ln–N bonds in these materials allow for analysis of lanthanide contraction effects on both local and supramolecular assembly across the majority of the Ln(III) series.

Experimental section

Materials and methods

$Ce(NO_3)_3{\cdot}6H_2O$ (Sigma Aldrich, 99%), $Pr(NO_3)_3{\cdot}6H_2O$ (Strem Chemicals, 99.9%) $Nd(NO_3)_3{\cdot}6H_2O$ (Sigma Aldrich, 99.9%), $Sm(NO_3)_3{\cdot}6H_2O$ (Strem Chemicals, Alfa Aesar, 99.9%) $Eu(NO_3)_3{\cdot}6H_2O$ (Alfa Aesar, 99.9%), $Ln(NO_3)_3{\cdot}xH_2O$ (where Ln = Gd–Lu, x = 1,5 or 6, Strem Chemicals, 99.9%), thiophene-2,5-dicarboxylic acid (Sigma Aldrich, 99%) and 2,2′:6′,2″-terpyridine (Alfa Aesar, 97%) were used for syntheses as received.

Synthesis

All compounds discussed herein were synthesized hydrothermally in a 23-mL Teflon-lined Parr bomb at an oven temperature of 180 °C and the protocol outlined below was deemed optimal for single-crystal growth.

A mixture of Ln^{3+} nitrate hexahydrate ($Ln(NO_3)_3{\cdot}xH_2O$, Ln = Ce–Lu, x = 1,5, or 6), thiophene-2,5-dicarboxylic acid ($C_6H_4SO_4$), 2,2′:6′,2″-terpyridine ($C_{15}H_{11}N_3$) and distilled water (molar ratio 1 : 2 : 1 : 826) was heated under autogenous pressure for either two or three days. Varying the reaction time was key for optimizing crystal growth. Initially all reaction vessels were heated for 72 hours, yet it was later discovered that single crystal quality was improved for Eu^{3+}, Dy^{3+}, and Lu^{3+} materials by heating the reaction vessels for only 48 hours. After either two or three days, the reaction vessels were allowed to cool to room temperature over approximately four hours. Colorless rectangular plate-like crystals were obtained from the bulk product after decanting the mother liquor, washing with distilled water and ethanol, and air-drying overnight at room temperature.

Although the Ce^{3+} and Pr^{3+} members of this series were successfully identified as structure type I *via* powder X-ray diffraction (PXRD) (Fig. S13 and S14, ESI†), we were unable to obtain suitable single crystals of these materials *via* the outlined protocol. Additional attempts were made to obtain suitable single crystals of these materials *via* alternative syntheses routes (solvothermal, slow evaporation, *etc.*), yet they were also unsuccessful. Further, with La^{3+}, we were not able to obtain suitable single crystals and were unsuccessful in identifying our final product *via* PXRD.

Characterization

X-ray structure determination. Single crystals from each bulk sample were isolated and mounted on MiTeGen micromounts. Reflections were collected at room temperature (293 (2) K) using MoKα (λ = 0.71073 Å) radiation and 0.5° ω scans on a Bruker SMART diffractometer furnished with an APEX II CCD detector. Data sets were integrated using the SAINT software package[61] that is a part of the APEX II software suite[62] and absorption corrections were applied *via* SADABS.[63] Non-merohedral twinning in **1**, **8**, **11**, (two components), and **6** (three components) was accounted for with TWINABS.[64] Compounds **1**, **3–5**, and **7–11** were solved *via* direct methods using SIR 92[65] whereas compounds **2** and **6** were solved *via* the Patterson Method (SHELXS-2014).[66] All compounds (**1–11**)

 This journal is © The Royal Society of Chemistry 2015

Published on 05 August 2015. Downloaded by UNIVERSIDAD ESTADUAL DE CAMPINAS on 05/05/2016 19:33:05.

were refined using *SHELXL-2014* within the *WinGX*[89] software suite. In each structure, all non-hydrogen atoms were located *via* difference Fourier maps and refined anisotropically. Aromatic hydrogen atoms on the terpy and 2,5-TDC ligands were placed at their idealized positions and allowed to ride on the coordinates of their parent carbon atom ((U_{iso}) fixed at $1.2U_{eq}$). The hydrogen atoms on the bound water molecules in compounds **1–7** and on the lattice water molecules in compounds **3–10** could not be located and were thus not modeled. Hydrogen atoms on the lattice water molecules in **11** were located but were not included in the final model as they failed to refine satisfactorily. Positional disorder in the 2,5-TDC ligand of **3**, **4** (O1) and **7** (C46) was restrained *via* the ISOR command with an uncertainty value of either 0.01 (**3**) or 0.005 (**4**, **7**). In **1–11**, PLATON[67] suggested that there was additional pseudo-symmetry not accounted for in the space group $P\bar{1}$. We manually tried to solve each structure in the space groups *Pm*, *P*2, and *P*2/*m*. We could not obtain adequate structure solutions/refinements in any of these higher symmetry space groups and we view these findings as indicative that our selection of $P\bar{1}$ as the space group for compounds **1–11** is correct. Data collection and refinement details for compounds **1–11** are included in Table 1.

Powder X-ray diffraction. Powder X-ray diffraction (PXRD) data were collected on the bulk reaction product of compounds **1–11** (Fig. S2–S12, ESI†), as well as the analogous Ce^{3+} and Pr^{3+} materials (**12** and **13**), and were used to examine the bulk purity of each sample. All data were collected on a Rigku Miniflex (Cu Kα, 2θ = 3–60°) and were analyzed using the JADE software package.[68] The bulk products of **3–8** co-formed with a second inorganic phase, a well-known Ln^{3+}-25TDC MOF ($[Ln_2(2,5\text{-TDC})_3(H_2O)_4]_n$ where Ln = Nd^{3+}–Er^{3+}).[38,43,44,69–71] Attempts to synthesize only **3–8** as a pure phase, resulted in either a biphasic mixture or a pure sample of the corresponding Ln^{3+}-25TDC MOF. Representative single crystal XRD data on the Eu-25TDC MOF can be found in the Table S1 and Fig. S1, ESI,† and thus further spectroscopic characterization of **3–8** were not performed.

Luminescence measurements. Visible and near-IR solid-state luminescence for compounds **1**, **2**, and **13** were obtained on a Fluorolog-3 spectrofluorimeter (Horiba FL3-22-iHR320). Emission and excitation spectra were recorded using a 450 W Xenon lamp ozone free (Ushio) as the excitation source. UV-Vis excitation spectra were corrected in real time according to the lamp intensity and optical system using a silicon diode as a reference. Visible emission spectra for **2** were carried out using the front face mode and corrected according to the optical system and the photomultiplier (Hamamatsu R928P) response. Near-IR emission spectra for **1**, **2**, and **13** were obtained using the iHR320 emission monochromator and a Hamamatsu H10330A-75 photomultiplier. Data were manipulated using the FluoroEssence software package and the Origin 8.1 software program.

Near-IR photophysical data for compound **10** were obtained on JobinYvon-Horiba Fluorolog-3 spectrometer fitted with Hamamatsu R5509-73 detector (cooled to −80 °C using C9940 housing). Lifetime data for **10** were obtained on a JobinYvon-Horiba Fluorolog-3 spectrometer fitted with a JY TBX picosoeconds photodetection module and a Continuum Minilite Nd:YAG pulsed laser source configured for 355 nm output. The luminescent lifetime profile of **10** was obtained using the JobinYvon FluoroHub single photon counting module and the data were fit using the provided DAS6 deconvolution software.

Results

Description of the structures

X-ray crystallography analyses revealed three unique structure types in this family of Ln-25TDC-terpy materials as detailed in Table 2.

A representative from each of the observed examples (**2**, **6** and **11**) will be discussed in detail.

$[Ln_2(C_{15}H_{11}N_3)_2(C_6H_4O_4S)_3(H_2O)_2]$ where (Ln = Ce^{3+}, Pr^{3+}, Nd^{3+}, and Sm^{3+}) (1–2, 12–13)-structure type I

Single crystal X-ray diffraction reveals that compounds **1** and **2** are isomorphous and crystallize in the space group $P\bar{1}$ and additionally, powder X-ray diffraction confirmed that compounds **12** and **13** are also isomorphous with **1** and **2**. As such, the Sm^{3+} compound (**2**) will be used as a representative example and described here in detail. The asymmetric unit of **2** contains two crystallographically unique nine-coordinate Sm^{3+} ions with molecular geometries that can be described as tricapped trigonal prismatic. Each Sm^{3+} metal center is coordinated by six oxygen atoms, five from 2,5-TDC ligands and one from a bound water molecule, as well as three nitrogen atoms from a tridentate terpy moiety. (Fig. 1) The Sm^{3+} cations of **2** are tethered *via* a μ_4–η^2:η^2 TDC linker (O9–O12) to result in binuclear secondary building units (SBUs), with bond distances of 2.358(2) Å (Sm2–O9), 2.350(2) Å (Sm2–O10), 2.364(2) Å (Sm1–O11), and 2.451(2) Å (Sm1–O12), respectively. (Fig. 1) The binuclear SBUs of **2** are further connected along the [100] direction by μ_3–η^2:η^1 TDC linkers (O1, O3, O4 and O5, O6, O7) at an average distance of 2.473 Å to generate a 2D sheet. Both unique Sm^{3+} metal centers are bound to chelating terpy molecules through their three nitrogen atoms (N1–N6) at an average Sm–N bond distance of 2.594 Å and the coordination of these capping ligands serves to truncate one side of the Sm^{3+} coordination sphere of both Sm1 and Sm2, thereby limiting further connectivity. The coordination sphere of both Sm1 and Sm2 is completed by bound water molecules (OW1 and OW2) with respective bond distances of 2.603(2) Å (Sm1–OW1) and 2.646 (3) Å (Sm2–OW2).

The 2D sheets of **2** feature one-dimensional rhomboidal voids with dimensions of *ca.* 6.80 Å × 6.00 Å, as determined from the shortest O–O atom position distances (O10–O12 and O1–O7), along the [100] direction. (Fig. 2) Each void space has a volume of 45 $Å^3$ (*via* PLATON) and the voids of each sheet of **2** align to form channels free of solvent water molecules. The sheets of **2** are assembled into a supramolecular 3D network *via* the chelating terpy ligands, which interact with

Published on 05 August 2015. Downloaded by UNIVERSIDAD ESTADUAL DE CAMPINAS on 05/05/2016 19:33:05.

Table 1 Crystallographic data for compounds **1–11**

	1	**2**	**3**	**4**
Chem formula	$C_{48}H_{32}S_3N_6O_{14}Nd_2$	$C_{48}H_{32}S_3N_6O_{14}Sm_2$	$C_{48}H_{32}S_3N_6O_{14}Eu_2$	$C_{48}H_{32}S_3N_6O_{14}Gd_2$
Formula weight	1301.45	1313.67	1316.89	1327.47
Cryst system	Triclinic	Triclinic	Triclinic	Triclinic
Space group	$P\bar{1}$	$P\bar{1}$	$P\bar{1}$	$P\bar{1}$
a (Å)	11.305(2)	11.2941(3)	9.990(6)	9.998(6)
b (Å)	14.497(3)	14.5181(4)	14.334(7)	14.333(6)
c (Å)	16.410(3)	16.4145(4)	18.575(7)	18.542(7)
α (°)	70.12(3)	70.151(4)	110.283(6)	110.286(5)
β (°)	89.32(3)	89.570(5)	99.536(5)	99.753(4)
γ (°)	73.80(3)	74.061(5)	99.030(5)	98.966(5)
V (Å^3)	2418.7(10)	2423.28(14)	2393.0(2)	2389.0(2)
Z	2	2	2	2
T (K)	293	293	293	293
λ (Mo Kα)	0.71073	0.71073	0.71073	0.71073
D_{calc} (g cm^{-3})	1.787	1.800	1.827	1.845
μ (mm^{-1})	2.327	2.603	2.803	2.958
R_{int}	0.0500	0.0379	0.0447	0.0343
R_1 [$I > 2\sigma(I)$]	0.0361	0.0326	0.0395	0.0299
wR_2 [$I > 2\sigma(I)$]	0.0892	0.0764	0.0976	0.0681
	5	**6**	**7**	**8**
Chem formula	$C_{48}H_{32}S_3N_6O_{14}Tb_2$	$C_{48}H_{32}S_3N_6O_{14}Dy_2$	$C_{48}H_{32}S_3N_6O_{14}Ho_2$	$C_{48}H_{32}S_3N_6O_{14}Er_2$
Formula weight	1330.81	1337.97	1342.83	1347.49
Cryst system	Triclinic	Triclinic	Triclinic	Triclinic
Space group	$P\bar{1}$	$P\bar{1}$	$P\bar{1}$	$P\bar{1}$
a (Å)	10.0155(8)	10.007(5)	10.0126(14)	11.2143(6)
b (Å)	14.3215(11)	14.298(6)	14.278(2)	14.1588(7)
c (Å)	18.4709(15)	18.414(6)	18.369(3)	16.1350(8)
α (°)	110.097(10)	109.983(5)	109.892(4)	109.045(9)
β (°)	99.868(11)	99.963(4)	99.969(4)	94.266(8)
γ (°)	99.041(10)	99.123(4)	99.169(3)	99.948(9)
V (Å^3)	2382.6(4)	2370.3(17)	2363.5(6)	2361.6(3)
Z	2	2	2	2
T (K)	293	293	293	293
λ (Mo Kα)	0.71073	0.71073	0.71073	0.71073
D_{calc} (g cm^{-3})	1.855	1.875	1.887	1.895
μ (mm^{-1})	3.151	3.336	3.532	3.738
R_{int}	0.0330	0.0345	0.0588	0.0357
R_1 [$I > 2\sigma(I)$]	0.0335	0.0319	0.0441	0.0470
wR_2 [$I > 2\sigma(I)$]	0.0831	0.0706	0.0916	0.1007

	9	**10**	**11**
Chem formula	$C_{48}H_{32}S_3N_6O_{14}Tm_2$	$C_{48}H_{32}S_3N_6O_{14}Yb_2$	$C_{48}H_{32}S_3N_6O_{14}Lu_2$
Formula weight	1350.83	1359.05	1362.91
Cryst system	Triclinic	Triclinic	Triclinic
Space group	$P\bar{1}$	$P\bar{1}$	$P\bar{1}$
a (Å)	11.1911(7)	11.165(5)	11.1563(4)
b (Å)	14.1360(9)	14.113(7)	14.0857(5)
c (Å)	16.1242(10)	16.117(8)	16.1004(6)
α (°)	108.997(11)	108.934(7)	108.865(3)
β (°)	94.492(10)	94.613(6)	94.701(2)
γ (°)	99.700(12)	99.554(6)	99.566(2)
V (Å^3)	2353.0(3)	2344.0(2)	2335.79(15)
Z	2	2	2
T (K)	293	293	293
λ (Mo Kα)	0.71073	0.71073	0.71073
D_{calc} (g cm^{-3})	1.907	1.925	1.938
μ (mm^{-1})	3.956	4.175	4.413
R_{int}	0.0192	0.0461	0.0537
R_1 [$I > 2\sigma(I)$]	0.0165	0.0435	0.0343
wR_2 [$I > 2\sigma(I)$]	0.0404	0.1075	0.0634

one another *via* a pair of slightly offset π–π stacking interactions.[72] These non-covalent interactions are between the centroid (a calculated centroid, Cg, corresponds to the center of the aromatic ring) of the terpy moiety of one dimeric Sm^{3+} SBU with the periphery of a terpy molecule on the neighboring Sm^{3+} SBU. Centroids were calculated in the center of the aro-

 This journal is © The Royal Society of Chemistry 2015

Published on 05 August 2015. Downloaded by UNIVERSIDAD ESTADUAL DE CAMPINAS on 05/05/2016 19:33:05.

Table 2 Structural breakdown of Ln^{3+}-2,5-TDC-TPY family of materials (**1–13**). Boxes shaded orange correspond to structure type I, while green represents structure type II and blue corresponds to structure type III

La^{3+}	Ce^{3+}	Pr^{3+}	Nd^{3+}	Pm^{3+}	Sm^{3+}	Eu^{3+}	Gd^{3+}	Tb^{3+}	Dy^{3+}	Ho^{3+}	Er^{3+}	Tm^{3+}	Yb^{3+}	Lu^{3+}

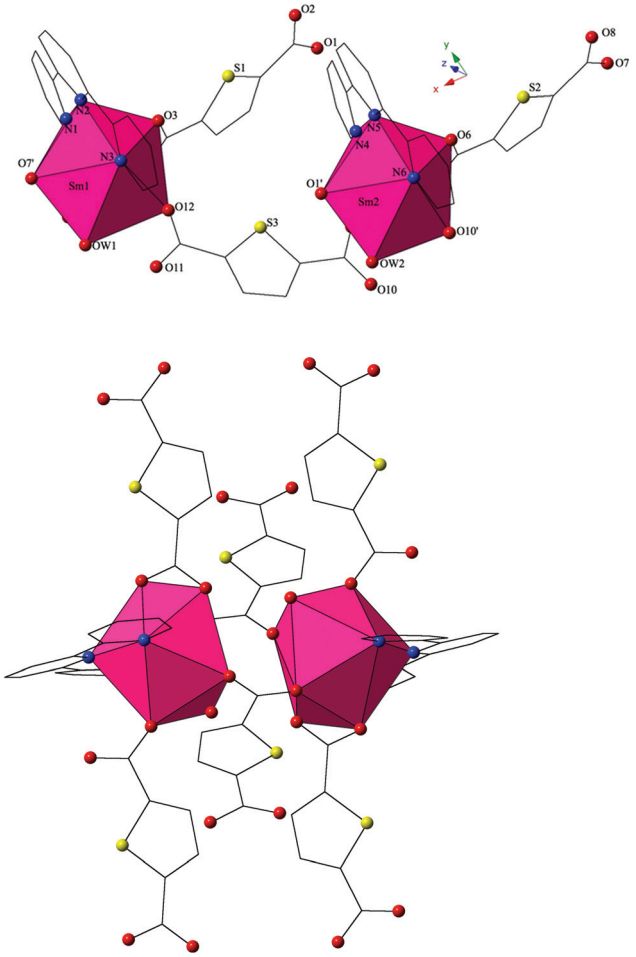

Fig. 1 (Top) Polyhedral representation of local structure of **2**. Pink polyhedra represent samarium metal centers, whereas spheres represent nitrogen (blue), oxygen (red), and sulfur (yellow). All H atoms have been omitted for clarity. (Bottom) Polyhedral representation of the binuclear SBU of **2**.

matic terpy rings participating in these interactions in order to obtain the linear distance (Cg···Cg) between the centroids as well as displacement perpendicular to the plane of the terpy rings for each of the unique π-stacks (Cg⊥···Cg⊥). Further, the angle (β) formed by the intersection of the line between centroids and the displacement perpendicular to the plane of the terpy rings was measured. The relevant distances and angles for these interactions are: Cg···Cg 3.694(2) Å, 3.805(2) Å; Cg⊥···Cg⊥ 3.3063(16) Å, 3.6669(17) Å; β = 26.47°, 15.46°.

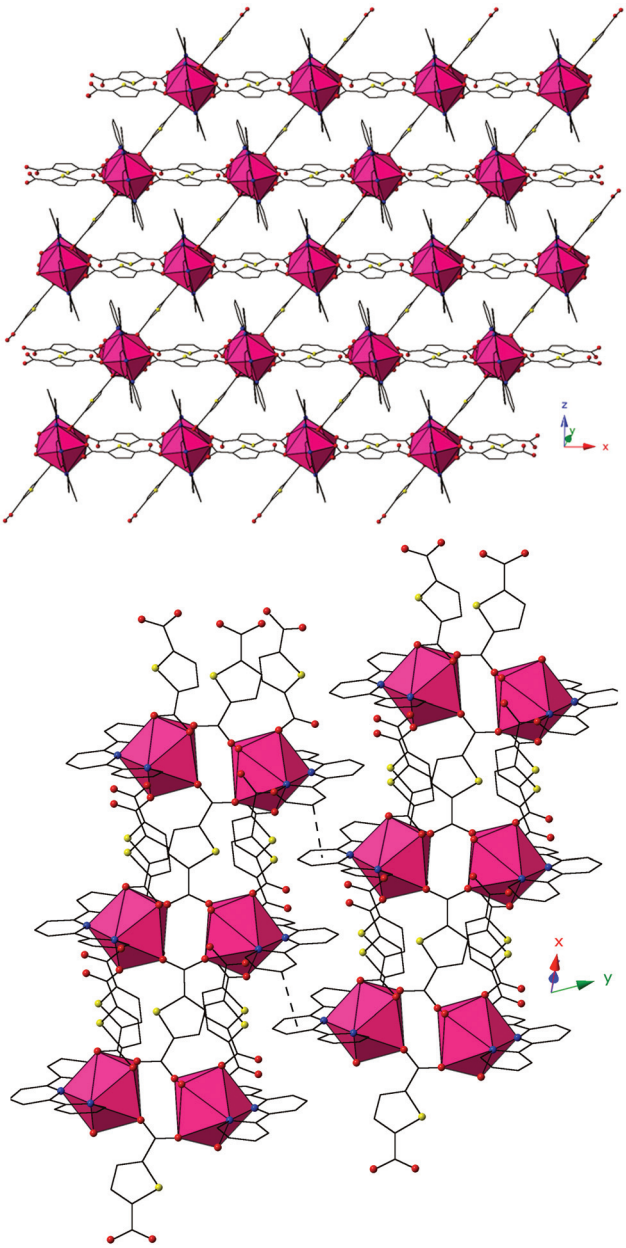

Fig. 2 (Top) 2D sheet of **2** viewed in the (101) plane. Pink polyhedra represent (SmO_6N_3) dimers, the SBUs that are linked into 2D sheets *via* TDC linkers. Each rhomboidal void is free of lattice molecules. (Bottom) **2** viewed down approximately the [100] direction. π–π interactions between terpy ligands that assemble 2D sheets of **2** into a supramolecular 3D network are shown.

Published on 05 August 2015. Downloaded by UNIVERSIDAD ESTADUAL DE CAMPINAS on 05/05/2016 19:33:05.

$[Ln_2(C_{15}H_{11}N_3)_2(C_6H_4O_4S)_3(H_2O)]\cdot H_2O$ where (Ln = Eu^{3+}, Gd^{3+}, Tb^{3+}, Dy^{3+}, and Ho^{3+}) (3–7)-structure type II

Single crystal X-ray diffraction analyses reveals compounds **3–7** are isomorphous and crystallize in the triclinic space group $P\bar{1}$. As such, only the Dy^{3+} compound (**6**) will be described herein, and as **6** features similar local coordination geometry to **2**, we will focus on the differences between structure types I and II rather than providing a detailed account of the first coordination sphere bonding environment (a complete list of all first coordination sphere bond distances for **3–7** can be found in the ESI, Tables S3 and S5†). The asymmetric unit of **6** consists of two crystallographically unique Dy^{3+} ions (Dy1 and Dy2). Dy1 is nine-coordinate, similar to the Sm^{3+} metal centers of **2**, and adopts a tricapped trigonal prismatic molecular geometry whereas Dy2 lacks a bound water molecule and thus the molecular geometry around the Dy^{3+} metal center is more accurately described as square antiprismatic. (Fig. 3) Like **2**, the Dy^{3+} cations are tethered *via* a μ_4–η^2:η^2 TDC linker to result in a 1D chain of binuclear secondary building units that is further connected into a 2D sheet *via* two crystallographically unique μ_3–η^2:η^1 TDC linkers, yet in **6** we now have two crystallographically unique binuclear SBUs rather than the one observed for **2**. (Fig. 3) Terpy molecules chelate both Dy1 and Dy2 and a bound water molecule completes the first coordination sphere of Dy1.

Looking at the global structure of the 2D sheet in **6**, we once again observe rhomboidal voids with dimensions of *ca.* 6.75 Å × 5.95 Å along approximately the [001] direction and similar to **2**, these voids align to form channels. (Fig. 4) Whereas in **2** each void space was empty, half of the voids in **6** contain lattice water molecules. These guest water molecules (OW2) participate in weak hydrogen bonding interactions with the 2D sheet of **6** by acting as both a hydrogen bond donor and acceptor in the well-known O–H···O and C–H···O

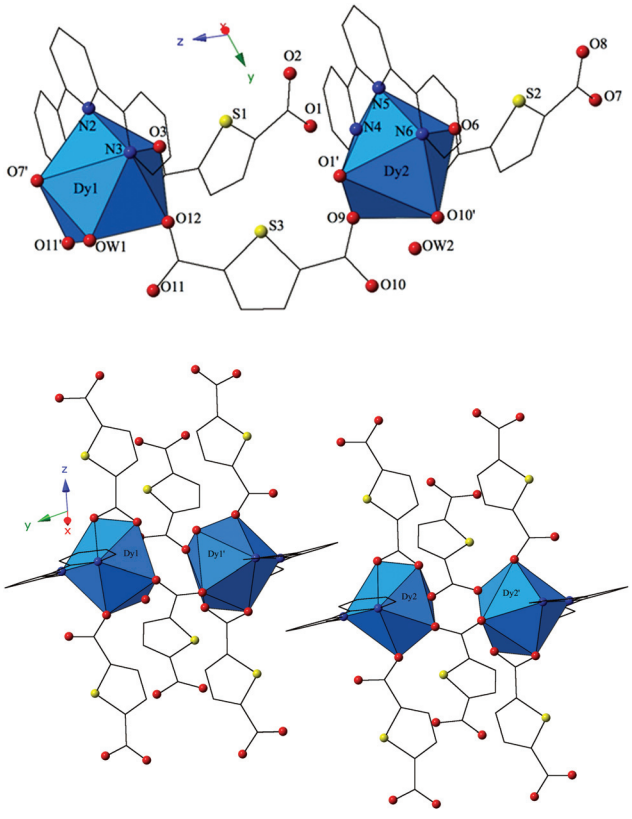

Fig. 3 (Top) Polyhedral representation of local structure of **6**. Blue polyhedra represent Dy^{3+} metal centers. All H atoms have been omitted for clarity. (Bottom) Polyhedral representation of binuclear SBUs of **6**. All H atoms and lattice water molecules have been omitted for clarity.

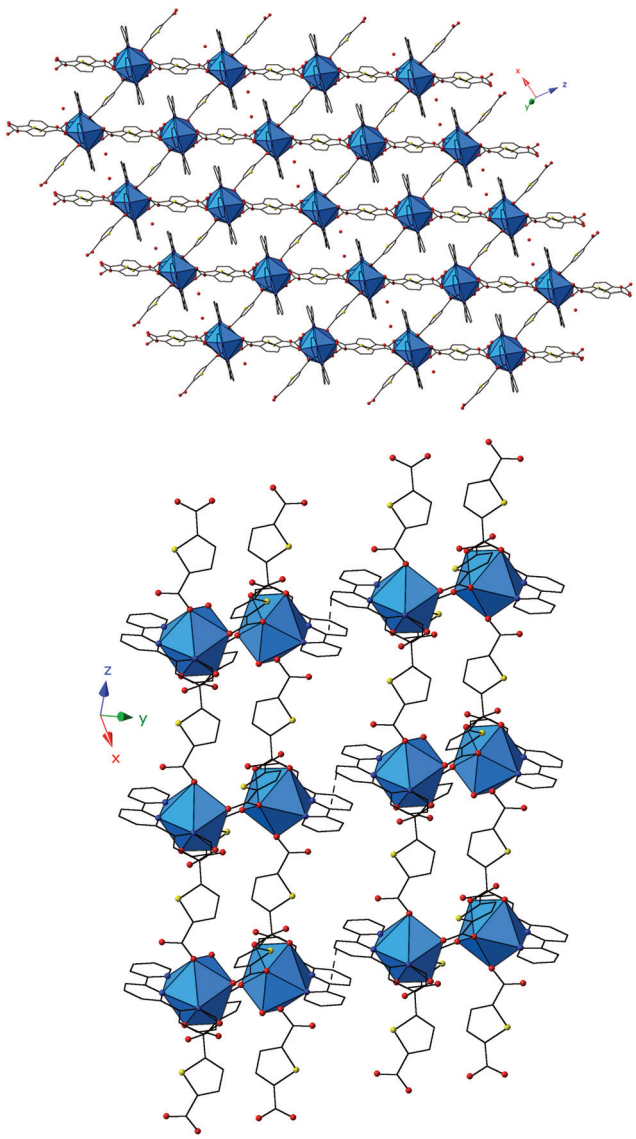

Fig. 4 (Top) 2D sheet of **6** viewed in approximately the (101) plane. Blue polyhedra represent (DyO_5N_3) and (DyO_6N_3) dimers, the SBUs that are tethered into 2D sheets *via* TDC linkers. Alternating rows of rhomboidal voids contain two lattice water molecules (red spheres). (Bottom) **6** viewed down the [001] direction. π–π interactions between terpy ligands that tether 2D sheets of **6** are shown. All lattice water molecules have been omitted for clarity.

This journal is © The Royal Society of Chemistry 2015

Published on 05 August 2015. Downloaded by UNIVERSIDAD ESTADUAL DE CAMPINAS on 05/05/2016 19:33:05.

synthons.[73–76] The interactions are between OW2 and O5 (the O–H···O synthon) at a distance of 2.793(9) Å and OW2 and C35 (the C–H···O synthon) at a distance 3.341(10) Å. Similar to **2**, the sheets of **6** are linked to form a supramolecular 3D network *via* a pair of slightly offset π–π interactions that are between the centroid of the terpy moiety of one dimeric Dy^{3+} SBU with the periphery of a terpy molecule on the neighboring Dy^{3+} SBU. The relevant distances and angles for these interactions are: Cg···Cg 3.690(3) Å, 3.779(3) Å; Cg⊥···Cg⊥ 3.2920 (18) Å, 3.5788(19) Å; β = 26.85°, 18.74°.

$[Ln_2(C_{15}H_{11}N_3)_2(C_6H_4O_4S)_3]\cdot 2H_2O$ where (Ln = Er^{3+}, Tm^{3+}, Yb^{3+}, and Lu^{3+}) (8–11)-structure type III

Single crystal X-ray diffraction analyses reveals compounds **8–11** are isomorphous and crystallize in the triclinic space group $P\bar{1}$. As such, only the Lu^{3+} compound (**11**) will be described herein, and as compound **11** features similar local coordination geometry to both **2** and **6**, we will focus on the differences between structure type III and structure types I and II rather than providing a detailed account of the first coordination sphere bonding environment. (A complete list of all first coordination sphere bond distances for **8–11** can be found in the Tables S4 and S5, ESI†) The asymmetric unit of **11** consists of two crystallographically unique Lu^{3+} ions (Lu1 and Lu2), which are both eight-coordinate, similar to Dy2 of **6**, and adopt molecular geometries that can be described as square antiprismatic. (Fig. 5) While both Lu1 and Lu2 lack a bound water molecule in their first coordination sphere, which differs from **2** and **6**, we once again observe Ln^{3+} cations (in this case Lu^{3+}) that are tethered *via* a μ_4–η^2:η^2 TDC linker to result in a chain of binuclear secondary building units. (Fig. 5) Further, the chains of **11** are connected into a 2D sheet *via* two crystallographically unique μ_3–η^2:η^1 TDC linkers and dimensionality is limited by chelating terpy molecules, which cap each of the Lu^{3+} metal centers.

Similar to both structure types I and II, the global structure of **11** features a 2D sheet highlighted by rhomboidal channels with dimensions of *ca.* 6.70 Å × 5.90 Å along approximately the [100] direction. (Fig. 6) Whereas in **2** we observed voids that are empty and in **6** we noted that half feature lattice water molecules, in **11** we now have two lattice water molecules (OW1 or OW2) in each rhomboidal void of the 2D sheet. Both of these lattice water molecules participate in weak hydrogen bonding interactions with the 2D sheet of **11**. Similar to **6**, the lattice water molecules in the voids of **11** act as both hydrogen bond donors and acceptors and participate in two hydrogen bonding synthons (O–H···O and C–H···O). OW1 interacts with the carboxylate oxygen O1 at a distance of 2.870(10) Å and with C23 at distance of 3.256(11) Å. Similarly, OW2 interacts with O5 and C2 at distances of 2.753(7) Å and 3.349(9) Å, respectively. The 2D sheet of **11** is assembled into supramolecular 3D network in the same manner as both **2** and **6**, through a pair of slightly offset π–π interactions between the centroid of the terpy moiety of one dimeric Lu^{3+} SBU with the periphery of a terpy molecule on the neighboring Lu^{3+} SBU. The relevant distances and angles for these interactions are: Cg···Cg 3.712(3) Å, 3.830(3) Å; Cg⊥···Cg⊥ 3.359(2) Å, 3.525(2) Å; β = 23.80°, 29.54°.

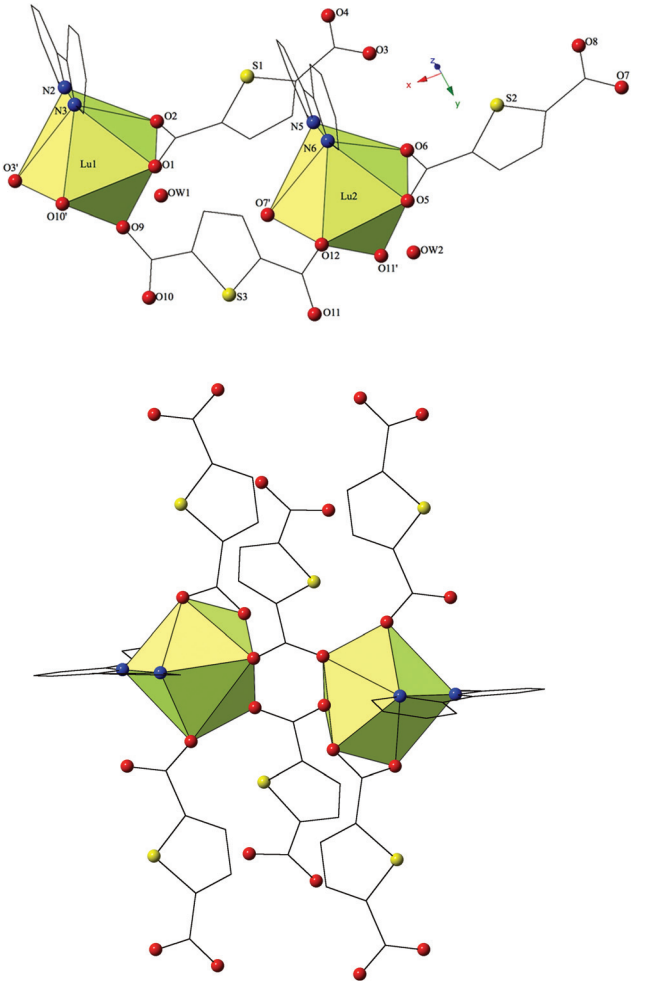

Fig. 5 (Top) Polyhedral representation of local structure of **11**. Yellow polyhedra represent Lu^{3+} metal centers. All H atoms have been omitted for clarity. (Bottom) Polyhedral representation of the binuclear SBU of **11**. All H atoms and lattice water molecules have been omitted for clarity.

Structural discussion

While there have been a number of studies on Ln^{3+}-2,5-TDC hybrids,[37–44] this is the first series of Ln^{3+}-2,5-TDC materials where one can evaluate the effects of the addition of a co-ligand (terpy) on both the local structures and their subsequent modes of supramolecular assembly. We recently examined the evolution of local coordination geometries and modes of supramolecular assembly in a series of molecular Ln^{3+}-*p*-chlorobenzoic acid-terpy materials,[49] and herein we extend this concept to coordination polymers, explored *via* the family of Ln^{3+}-2,5-TDC-terpy hybrids described throughout.

In **1–11**, each Ln^{3+} metal center is chelated by a tridentate terpy molecule, linked *via* a μ_4–η^2:η^2 TDC to result in a bi-

Published on 05 August 2015. Downloaded by UNIVERSIDAD ESTADUAL DE CAMPINAS on 05/05/2016 19:33:05.

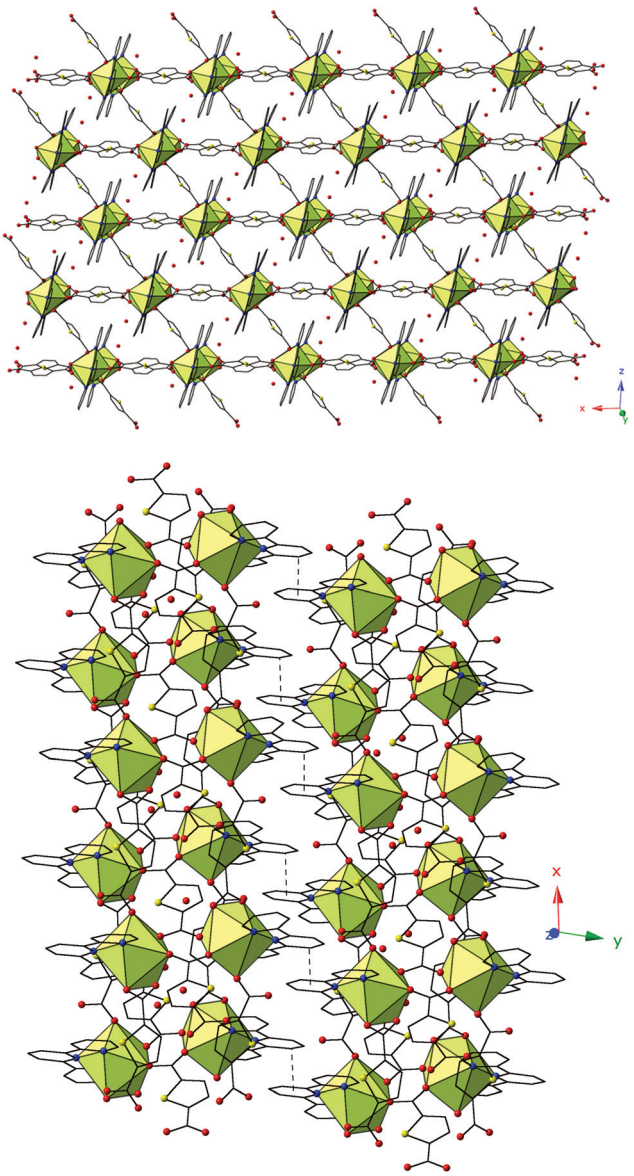

Fig. 6 (Top) 2D sheet of **11** viewed in the (101) plane. Yellow polyhedra represent (LuO_5N_3) dimers, the SBU that are assembled into 2D sheets *via* TDC linkers. Each rhomboidal void contains two lattice water molecules (red spheres). (Bottom) **11** viewed down the [100] direction. π–π interactions between terpy ligands that link 2D sheets of **11** are shown. All lattice water molecules have been omitted for clarity.

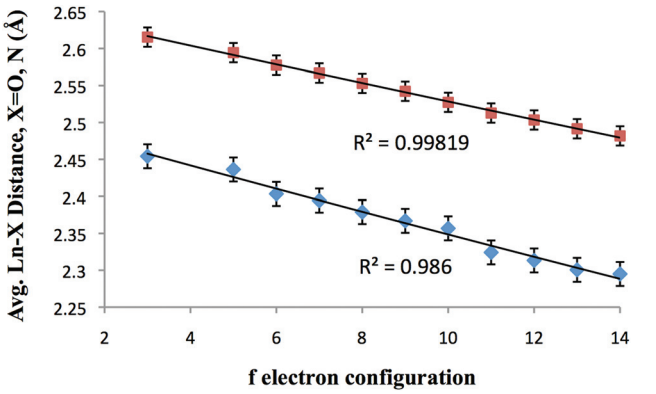

Fig. 7 Average Ln–O (blue diamonds) and Ln–N (red squares) bond distances (Å) *vs.* the f electron configuration for **1–11** (Error bars represent propagated uncertainty of avg. Ln–O and Ln–N distances).

nuclear SBU and then further connected to two unique TDC ligands that have adopted the μ_3-η^2:η^1 coordination mode to form a 2D sheet. The Ln^{3+} cations of **1** and **2** also feature a bound water molecule in their first coordination sphere, whereas **3–7** only feature a bound water molecule on one Ln^{3+} cation due to the effects of the smaller ionic radii of the corresponding Ln^{3+} metal centers. For compounds **8–11**, all bound water molecules have been crowded out of the Ln^{3+} first coordination sphere and one observes two guest water molecules in each void of the 2D sheet as highlighted in Fig. 6. The evolution of the location of the water molecules (OW1, OW2) from the first coordination sphere to decorating the rhomboidal voids of the 2D sheet as one moves across the Ln^{3+} series corresponds with observed changes in both local coordination geometry and the corresponding modes of assembly. Whereas the former is a relatively straightforward observation that can be easily explained by the lanthanide contraction, it is interesting that the number of water molecules, regardless of location, is consistent in structure types I, II, and III. The changes in modes of assembly of the 2D sheets are a more subtle manifestation, as the overall global structure of **1–11** remains constant. In **1** and **2**, assembly is limited to slightly offset π–π interactions that link the 2D sheet into a supramolecular 3D network. In **3–7**, we once again observe π–π interactions, of similar magnitude to those in **1** and **2** (ESI, Table S6†), and additionally we now note hydrogen bonding interactions in every other channel where water molecules now reside. These hydrogen-bonding interactions, a combination of the well-known O–H···O and C–H···O synthons, decorate the covalent bonding network that links the 2D sheet. Compounds **8–11** feature both π–π and hydrogen-interactions as described above and as water molecules are now found only in the lattice, we now observe hydrogen bonding interactions in every channel, rather than in every other as was observed in **3–7**.

As the location of the water molecules (OW1, OW2) is the only change between structure types I, II, and III, we can use the Ln–O (carboxylate) and Ln–N bond length information (Tables S2–S5, ESI†) to explore the effect of the lanthanide contraction in Ln^{3+}-25TDC-terpy hybrid materials. A plot of average Ln–O (carboxylate) and Ln–N bond distances *versus* f-element electronic configuration is shown in Fig. 7. We observe that the decrease in both sets of bond distances is best modeled by a quadratic decay, consistent with the earlier results of Quadrelli,[77] Ibers and colleagues[78] and Raymond *et al.*[79]

Luminescence

Room temperature solid-state photoluminescent spectra were obtained for compounds **1**, **2**, the isomorphous Pr^{3+} material

 This journal is © The Royal Society of Chemistry 2015

Published on 05 August 2015. Downloaded by UNIVERSIDAD ESTADUAL DE CAMPINAS on 05/05/2016 19:33:05.

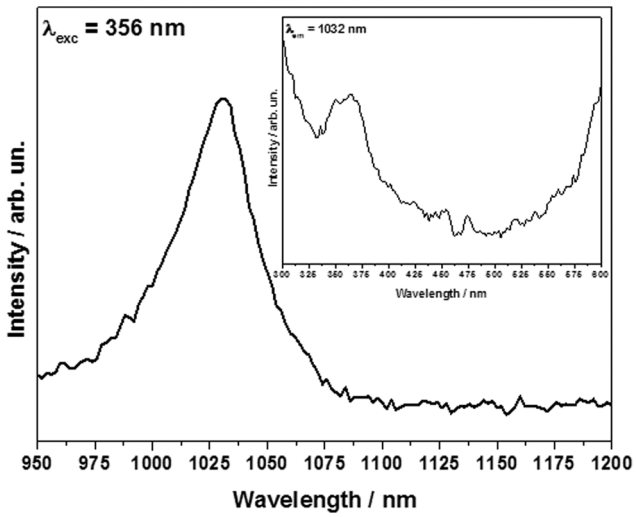

Fig. 8 Room temperature, solid state, near-IR emission spectrum for Pr^{3+} compound **13**. Inset: excitation spectrum for **13**.

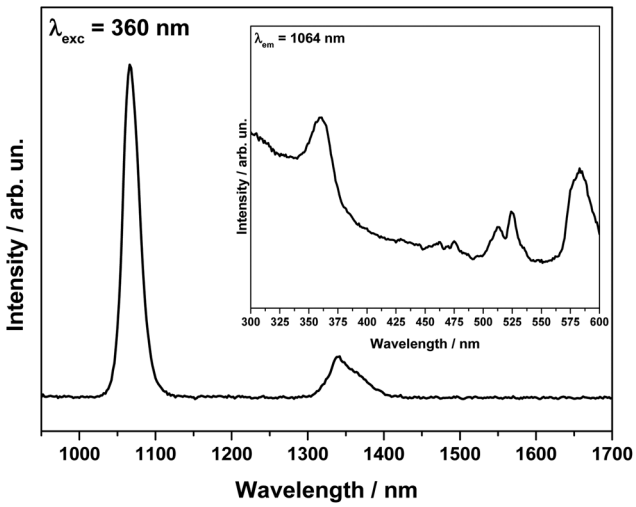

Fig. 9 Room temperature, solid state, near-IR emission spectrum for Nd^{3+} compound **1**. Inset: excitation spectrum for **1**.

(**13**), and **10**. Compounds **3–8** co-formed with a second inorganic species, that has been previously characterized, and as a result luminescent measurements were not taken. Compounds were excited at wavelengths corresponding to the absorption maxima of the terpy ligand which functions as the antenna in these coordination polymers.

For the Pr^{3+} material (**13**), luminescence was investigated in both the visible and near-IR regions. Upon excitation at the absorption maxima of the terpy ligand (356 nm) no luminescence was observed in the visible region while one band at 1030 nm (the $^1D_2 \rightarrow {}^3F_4$ transition) was observed in the near-IR region. (Fig. 8) Pr^{3+} has two emitting levels with the $^3P_0$ level of praseodymium at *ca.* 21 390 cm^{-1} and the $^1D_2$ level at *ca.* 16 800 cm^{-1},[80] while the triplet state energy level of 2,2′:6′,2″-terpyridine was measured at 22 962 cm^{-1}. According to Latva's energy match principle, energy transfer efficiency is optimized when differences in triplet state energy are >2500 cm^{-1} and <*ca.* 5000 cm^{-1} in order to avoid both back energy transfer between the ligand triplet state and the lanthanide excited state and non-radiative decay.[60] The difference in the energy between the triplet state of the terpy ligand and the $^3P_0$ state of Pr^{3+} is 1572 cm^{-1} (the difference between terpy and the $^1D_2$ level is 6162 cm^{-1}) so energy transfer from ligand to Pr^{3+} excited states should happen, even if the process is somewhat inefficient. Hasegawa *et al.*[81] have shown that energy transfer from antenna ligands to Pr^{3+} first proceeds through the non-emitting $^1I_6$ and $^3P_1$ states before reaching the emitting $^3P_0$ state. As the energy gap between the $^3P_0$ state and the terpy ligand triplet state was less than the 2500 cm^{-1} recommended by Latva's rules,[60] proceeding first through higher energy states would enhance back energy transfer pathways and provide easier means for non-radiative deactivation. Both of the unique Pr^{3+} metal centers also contain a coordinated water molecule in their first coordination sphere so it is perhaps not surprising that praseodymium luminescence is completely absent in the visible region. Moreover, reports of Pr^{3+} luminescence in both the visible and near-IR regions are relatively rare.[82–84]

The near-IR luminescence spectrum of **1** was collected at an excitation wavelength of 360 nm and features two spectral bands at *ca.* 1066 nm and 1342 nm corresponding to the $^4F_{3/2} \rightarrow {}^4I_J$ (J = 11/2, 9/2) transitions of Nd(III), respectively. (Fig. 9) The third characteristic transition of Nd(III) at *ca.* 880 nm ($^4F_{3/2} \rightarrow {}^4I_{9/2}$) was not observed as it fell below the lower limit of the detector used for NIR measurements.

For **2** (Sm^{3+}), characteristic emission was observed in both the visible and near-IR regions. The visible luminescence spectrum for **2** was collected at an excitation wavelength of 352 nm

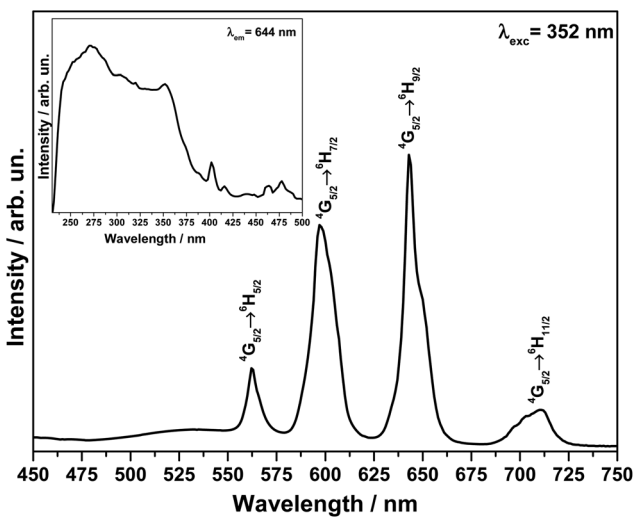

Fig. 10 Room temperature, solid state, visible emission spectrum for Sm^{3+} compound **2**. Inset: excitation spectrum for **2**.

Published on 05 August 2015. Downloaded by UNIVERSIDAD ESTADUAL DE CAMPINAS on 05/05/2016 19:33:05.

and features the characteristic $^4G_{5/2} \rightarrow {}^6H_J$ (J = 5/2, 7/2 and 9/2) transitions of Sm^{3+} at *ca.* 562 nm, 597 nm and 642 nm, respectively. (Fig. 10) The most intense of the three visible transitions is the hypersensitive $^4G_{5/2} \rightarrow {}^6H_{9/2}$ which, along with the $^4G_{5/2} \rightarrow {}^6H_{7/2}$ magnetic-dipole transition, are responsible for the orange-red color of Sm^{3+} emission.[85]

The near-IR luminescence spectrum of **2** was collected at an excitation wavelength of 356 nm and features two characteristic bands at *ca.* 1024 nm and 1168 nm which correspond to the $^4G_{5/2} \rightarrow {}^6F_J$ (J = 7/2 and 9/2) of Sm^{3+} (Fig. 11). The $^4G_{5/2} \rightarrow {}^6F_{5/2}$ transition at *ca.* 950 nm, which is typically the most intense Sm^{3+} transition in the near-IR region,[86] was not observed as it fell below the lower limit of the detector used for NIR measurements.

The near-IR luminescence spectrum of **10** was collected at an excitation wavelength 355 nm and features one spectral band at 979 nm corresponding to the characteristic $^2F_{5/2} \rightarrow {}^2F_{7/2}$ transition of Yb^{3+}. (Fig. 12) An unresolved shoulder peak at approximately 999 nm is the likely result of unresolved M_J splitting of the emitting and/or fundamental states of Yb^{3+}, which can be induced by ligand field effects.[87,88]

Further, the luminescent lifetime of **10** was measured at an excitation wavelength of 355 nm at room temperature and the corresponding decay curve is shown in Fig. 12. The resulting lifetime of the Yb^{3+} compound **10** was found to be 9.85 μs after a mono-exponential fitting of the decay curve. The long lifetime value is certainly consistent with a well encapsulated Yb^{3+} center that does not incorporate a coordinated water molecule.

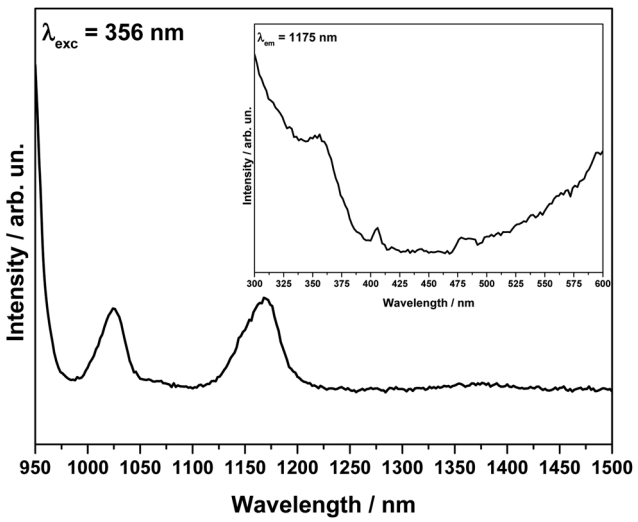

Fig. 11 Room temperature, solid state, near-IR emission spectrum for Sm^{3+} compound **2**. Inset: excitation spectrum for **2**.

Conclusions

The synthesis and crystal structures of eleven lanthanide hybrid materials featuring thiophene-2,5-dicarboxylic acid and 2,2′:6′,2″-terpyridine obtained *via* hydrothermal reactions have been reported and their modes of supramolecular assembly and visible and near-IR luminescent properties (where possible) have been discussed. Additionally, two more Ln^{3+}-2,5-TDC-terpy hybrid materials have been identified *via* PXRD only and spectroscopically characterized. The lanthanide contraction plays a significant role in the structural changes and the resulting evolution in supramolecular assembly that is observed in structure types I, II, and III as one moves across the lanthanide series from Ce^{3+} to Lu^{3+}. Analysis of bond length data reveals a decay in both Ln–O and Ln–N distances that can be fitted quadratically. Follow up studies focusing on mixed-lanthanide ion 25-TDC-terpy hybrid materials are ongoing with the overall goal of exploring luminescent behavior in systems featuring multiple Ln^{3+} cations.

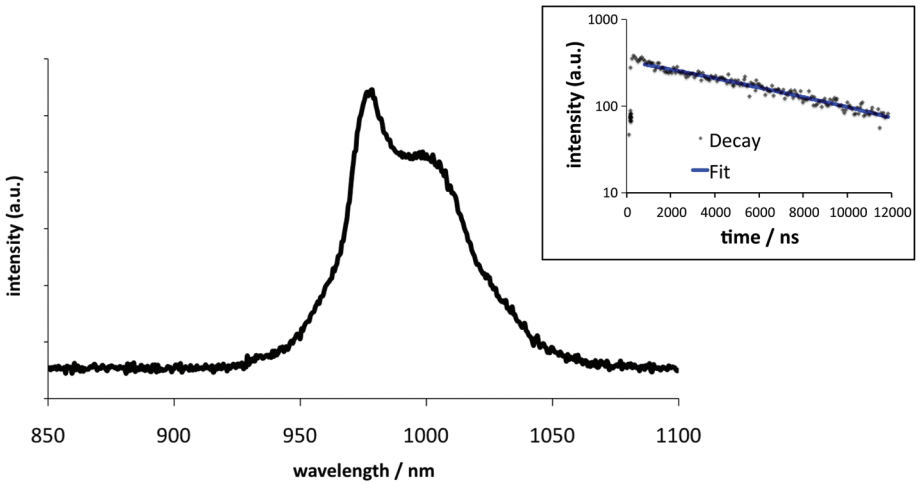

Fig. 12 Room temperature, solid state, near-IR emission spectrum for Yb^{3+} compound **10**. Inset: fitted luminescence decay for **10**.

 This journal is © The Royal Society of Chemistry 2015

Published on 05 August 2015. Downloaded by UNIVERSIDAD ESTADUAL DE CAMPINAS on 05/05/2016 19:33:05.

Conflict of interest

The authors declare no competing financial interest.

Acknowledgements

This material is based upon work supported as part of the Material Science of Actinides, an Energy Frontier Research Center funded by the U.S. Department of Energy, Office of Science, Office of Basic Energy Sciences, under Award Number DE-SC0001089. K. P. C. would also like to acknowledge George Washington University for a Presidential Merit Fellowship award. Additionally, C. H. Z. would like to acknowledge the CAPES Foundation for a CAPES Scholarship award (protocol number 4671120). F.A.S thanks the Laboratory of Advanced Optical Spectroscopy (LMEOA/IQ-UNICAMP/FAPESP Grant no. 2009/54066-7).

References

1 S. R. Batten, N. R. Champness, X.-M. Chen, J. Garcia-Martinez, S. Kitagawa, L. Ohrstrom, M. O'Keeffe, M. P. Suh and J. Reedijk, *CrystEngComm*, 2012, **14**, 3001–3004.
2 S. R. Batten, N. R. Champness, X.-M. Chen, J. Garcia-Martinez, S. Kitagawa, L. Öhrström, M. O'Keeffe, M. Paik Suh and J. Reedijk, *Pure Appl. Chem.*, 2013, **85**, 1715–1724.
3 T. M. Reineke, M. Eddaoudi, M. Fehr, D. Kelley and O. M. Yaghi, *J. Am. Chem. Soc.*, 1999, **121**, 1651–1657.
4 Y. Cui, Y. Yue, G. Qian and B. Chen, *Chem. Rev.*, 2012, **112**, 1126–1162.
5 Y. Hasegawa and T. Nakanishi, *RSC Adv.*, 2015, **5**, 338–353.
6 B. Chen, L. Wang, F. Zapata, G. Qian and E. B. Lobkovsky, *J. Am. Chem. Soc.*, 2008, **130**, 6718–6719.
7 Z. Guo, H. Xu, S. Su, J. Cai, S. Dang, S. Xiang, G. Qian, H. Zhang, M. O'Keeffe and B. Chen, *Chem. Commun.*, 2011, **47**, 5551–5553.
8 Y. Cui, B. Chen and G. Qian, *Coord. Chem. Rev.*, 2014, **273–274**, 76–86.
9 D.-X. Xue, A. J. Cairns, Y. Belmabkhout, L. Wojtas, Y. Liu, M. H. Alkordi and M. Eddaoudi, *J. Am. Chem. Soc.*, 2013, **135**, 7660–7667.
10 H. He, H. Ma, D. Sun, L. Zhang, R. Wang and D. Sun, *Cryst. Growth Des.*, 2013, **13**, 3154–3161.
11 S. Roy, A. Chakraborty and T. K. Maji, *Coord. Chem. Rev.*, 2014, **273–274**, 139–164.
12 F. Gándara, A. d. Andrés, B. Gómez-Lor, E. Gutiérrez-Puebla, M. Iglesias, M. A. Monge, D. M. Proserpio and N. Snejko, *Cryst. Growth Des.*, 2008, **8**, 378–380.
13 A. Corma, H. García and F. X. Llabrés i Xamena, *Chem. Rev.*, 2010, **110**, 4606–4655.
14 Y.-W. Ren, J.-X. Liang, J.-X. Lu, B.-W. Cai, D.-B. Shi, C.-R. Qi, H.-F. Jiang, J. Chen and D. Zheng, *Eur. J. Inorg. Chem.*, 2011, **2011**, 4369–4376.
15 S. M. F. Vilela, A. D. G. Firmino, R. F. Mendes, J. A. Fernandes, D. Ananias, A. A. Valente, H. Ott, L. D. Carlos, J. Rocha, J. P. C. Tome and F. A. Almeida Paz, *Chem. Commun.*, 2013, **49**, 6400–6402.
16 C. A. Black, J. S. Costa, W. T. Fu, C. Massera, O. Roubeau, S. J. Teat, G. Aromí, P. Gamez and J. Reedijk, *Inorg. Chem.*, 2009, **48**, 1062–1068.
17 J. Tian, B. Li, X. Zhang, X. Li, X. Li and J. Zhang, *Dalton Trans.*, 2013, **42**, 8504–8511.
18 W. Xu, Y. Zhou, D. Huang, W. Xiong, M. Su, K. Wang, S. Han and M. Hong, *Cryst. Growth Des.*, 2013, **13**, 5420–5432.
19 B. F. Abrahams, B. F. Hoskins, D. M. Michail and R. Robson, *Nature*, 1994, **369**, 727–729.
20 S. L. James, *Chem. Soc. Rev.*, 2003, **32**, 276–288.
21 C. Janiak, *Dalton Trans.*, 2003, 2781–2804.
22 N. Stock and S. Biswas, *Chem. Rev.*, 2011, **112**, 933–969.
23 T. Devic and C. Serre, *Chem. Soc. Rev.*, 2014, **43**, 6097–6115.
24 G. Férey, *Chem. Mater.*, 2001, **13**, 3084–3098.
25 M. Eddaoudi, D. B. Moler, H. Li, B. Chen, T. M. Reineke, M. O'Keeffe and O. M. Yaghi, *Acc. Chem. Res.*, 2001, **34**, 319–330.
26 N. W. Ockwig, O. Delgado-Friedrichs, M. O'Keeffe and O. M. Yaghi, *Acc. Chem. Res.*, 2005, **38**, 176–182.
27 B.-H. Ye, M.-L. Tong and X.-M. Chen, *Coord. Chem. Rev.*, 2005, **249**, 545–565.
28 M. D. Allendorf, C. A. Bauer, R. K. Bhakta and R. J. T. Houk, *Chem. Soc. Rev.*, 2009, **38**, 1330–1352.
29 M. D. Allendorf and V. Stavila, *CrystEngComm*, 2015, **17**, 229–246.
30 F. A. Almeida Paz, J. Klinowski, S. M. F. Vilela, J. P. C. Tome, J. A. S. Cavaleiro and J. Rocha, *Chem. Soc. Rev.*, 2012, **41**, 1088–1110.
31 J. Heine and K. Müller-Buschbaum, *Chem. Soc. Rev.*, 2013, **42**, 9232–9242.
32 L. V. Meyer, F. Schonfeld and K. Müller-Buschbaum, *Chem. Commun.*, 2014, **50**, 8093–8108.
33 K. Binnemans, *Chem. Rev.*, 2009, **109**, 4283–4374.
34 J.-C. G. Bünzli and C. Piguet, *Chem. Soc. Rev.*, 2005, **34**, 1048–1077.
35 S. I. Weissman, *J. Chem. Phys.*, 1942, **10**, 214–217.
36 J.-C. G. Bünzli, *Acc. Chem. Res.*, 2006, **39**, 53–61.
37 N. L. Rosi, J. Kim, M. Eddaoudi, B. Chen, M. O'Keeffe and O. M. Yaghi, *J. Am. Chem. Soc.*, 2005, **127**, 1504–1518.
38 J.-G. Wang, C.-C. Huang, X.-H. Huang and D.-S. Liu, *Cryst. Growth Des.*, 2008, **8**, 795–798.
39 L. F. Marques, M. V. dos Santos, S. J. L. Ribeiro, E. E. Castellano and F. C. Machado, *Polyhedron*, 2012, **38**, 149–156.
40 L. F. Marques, A. A. B. Cantaruti Júnior, S. J. L. Ribeiro, F. M. Scaldini and F. C. Machado, *Opt. Mater.*, 2013, **35**, 2357–2365.
41 P. J. Calderone, A. M. Plonka, D. Banerjee, Q. A. Nizami and J. B. Parise, *Solid State Sci.*, 2013, **15**, 36–41.
42 L. F. Marques, C. C. Correa, S. J. L. Ribeiro, M. V. dos Santos, J. D. L. Dutra, R. O. Freire and F. C. Machado, *J. Solid State Chem.*, 2015, **227**, 68–78.
43 W. Huang, D. Wu, P. Zhou, W. Yan, D. Guo, C. Duan and Q. Meng, *Cryst. Growth Des.*, 2009, **9**, 1361–1369.

Published on 05 August 2015. Downloaded by UNIVERSIDAD ESTADUAL DE CAMPINAS on 05/05/2016 19:33:05.

44 Z. Chen, B. Zhao, P. Cheng, X.-Q. Zhao, W. Shi and Y. Song, *Inorg. Chem.*, 2009, **48**, 3493–3495.
45 F. Allen, *Acta Crystallogr., Sect. B: Struct. Sci.*, 2002, **58**, 380–388.
46 C. M. MacNeill, C. S. Day, S. A. Gamboa, A. Lachgar and R. E. Noftle, *J. Chem. Crystallogr.*, 2010, **40**, 222–230.
47 Y.-G. Sun, B. Jiang, T.-F. Cui, G. Xiong, P. F. Smet, F. Ding, E.-G. Gao, T.-Y. Lv, K. Van den Eeckhout, D. Poelman and F. Verpoort, *Dalton Trans.*, 2011, **40**, 11581–11590.
48 C.-H. Zhan, F. Wang, Y. Kang and J. Zhang, *Inorg. Chem.*, 2012, **51**, 523–530.
49 K. P. Carter, S. J. A. Pope and C. L. Cahill, *CrystEngComm*, 2014, **16**, 1873–1884.
50 K. P. Carter, C. H. F. Zulato and C. L. Cahill, *CrystEngComm*, 2014, **16**, 10189–10202.
51 B. L. Chen, K. F. Mok, S.-C. Ng, Y.-L. Feng and S.-X. Liu, *Polyhedron*, 1998, **17**, 4237–4247.
52 B.-L. Chen, K.-F. Mok, S.-C. Ng and M. G. B. Drew, *New J. Chem.*, 1999, **23**, 877–883.
53 X.-Z. Sun, Z.-L. Huang, H.-Z. Wang, B.-H. Ye and X.-M. Chen, *Z. Anorg. Allg. Chem.*, 2005, **631**, 919–923.
54 H.-P. Jia, W. Li, Z.-F. Ju and J. Zhang, *Eur. J. Inorg. Chem.*, 2006, **2006**, 4264–4270.
55 H. He, D. Yuan, H. Ma, D. Sun, G. Zhang and H.-C. Zhou, *Inorg. Chem.*, 2010, **49**, 7605–7607.
56 S. G. Thangavelu, M. B. Andrews, S. J. A. Pope and C. L. Cahill, *Inorg. Chem.*, 2013, **52**, 2060–2069.
57 K. P. Carter and C. L. Cahill, *Inorg. Chem. Front.*, 2015, **2**, 141–156.
58 H.-R. Mürner, E. Chassat, R. P. Thummel and J.-C. G. Bunzli, *J. Chem. Soc., Dalton Trans.*, 2000, **0**, 2809–2816.
59 J. Lhoste, N. Henry, T. Loiseau, Y. Guyot and F. Abraham, *Polyhedron*, 2013, **50**, 321–327.
60 M. Latva, H. Takalo, V.-M. Mukkala, C. Matachescu, J. C. Rodríguez-Ubis and J. Kankare, *J. Lumin.*, 1997, **75**, 149–169.
61 *SAINT*, Bruker AXS Inc., Madison, WI, USA, 2007.
62 *APEX2*, Bruker AXS Inc., Madison, WI, USA, 2008.
63 *SADABS*, Bruker AXS Inc., Madison, WI, USA, 2008.
64 *TWINABS*, Bruker AXS Inc., Madison, WI, USA, 2008.
65 A. Altomare, G. Cascarano, C. Giacovazzo, A. Guagliardi, M. C. Burla, G. Polidori and M. Camalli, *J. Appl. Crystallogr.*, 1994, **27**, 435–435.
66 G. Sheldrick, *Acta Crystallogr., Sect. A: Found. Crystallogr.*, 2008, **64**, 112–122.
67 A. Spek, *Acta Crystallogr., Sect. D: Biol. Crystallogr.*, 2009, **65**, 148–155.
68 *JADE*, Materials Data Inc., Livermore, California, USA, 2003.
69 J. Ren, Y. Liu, Z. Chen, G. Xiong and B. Zhao, *Sci. China, Ser. B: Chem.*, 2012, **55**, 1073–1078.
70 X.-G. Du, J. Zhang and J.-J. Li, *Acta Crystallogr., Sect. E: Struct. Rep. Online*, 2012, **68**, m1024.
71 Y. Zhao and S.-H. Li, *Synth. React. Inorg. Met.-Org. Chem.*, 2015, **45**, 921–925.
72 C. Janiak, *J. Chem. Soc., Dalton Trans.*, 2000, 3885–3896.
73 G. R. Desiraju, *Angew. Chem., Int. Ed. Engl.*, 1995, **34**, 2311–2327.
74 G. R. Desiraju, *Acc. Chem. Res.*, 1996, **29**, 441–449.
75 G. R. Desiraju and T. Steiner, *The Weak Hydrogen Bond in Structural Chemistry and Biology*, Oxford University Press, Oxford, 1999.
76 G. R. Desiraju, *Acc. Chem. Res.*, 2002, **35**, 565–573.
77 E. A. Quadrelli, *Inorg. Chem.*, 2002, **41**, 167–169.
78 J. Yao, B. Deng, L. J. Sherry, A. D. McFarland, D. E. Ellis, R. P. Van Duyne and J. A. Ibers, *Inorg. Chem.*, 2004, **43**, 7735–7740.
79 M. Seitz, A. G. Oliver and K. N. Raymond, *J. Am. Chem. Soc.*, 2007, **129**, 11153–11160.
80 W. T. Carnall, P. R. Fields and K. Rajnak, *J. Chem. Phys.*, 1968, **49**, 4424–4442.
81 M. Hasegawa, A. Ishii and S. Kishi, *J. Photochem. Photobiol., A*, 2006, **178**, 220–224.
82 S. Quici, M. Cavazzini, G. Marzanni, G. Accorsi, N. Armaroli, B. Ventura and F. Barigelletti, *Inorg. Chem.*, 2005, **44**, 529–537.
83 A. de Bettencourt-Dias, P. S. Barber and S. Bauer, *J. Am. Chem. Soc.*, 2012, **134**, 6987–6994.
84 Z. Ahmed and K. Iftikhar, *J. Phys. Chem. A*, 2013, **117**, 11183–11201.
85 S. Biju, Y. K. Eom, J.-C. G. Bünzli and H. K. Kim, *J. Mater. Chem. C*, 2013, **1**, 6935–6944.
86 K. Lunstroot, P. Nockemann, K. Van Hecke, L. Van Meervelt, C. Görller-Walrand, K. Binnemans and K. Driesen, *Inorg. Chem.*, 2009, **48**, 3018–3026.
87 F. R. Gonçalves e Silva, O. L. Malta, C. Reinhard, H.-U. Güdel, C. Piguet, J. E. Moser and J.-C. G. Bünzli, *J. Phys. Chem. A*, 2002, **106**, 1670–1677.
88 L.-N. Sun, J.-B. Yu, G.-L. Zheng, H.-J. Zhang, Q.-G. Meng, C.-Y. Peng, L.-S. Fu, F.-Y. Liu and Y.-N. Yu, *Eur. J. Inorg. Chem.*, 2006, **2006**, 3962–3973.
89 L. Farrugia, *J. Appl. Crystallogr.*, 2012, **45**, 849–854.

This journal is © The Royal Society of Chemistry 2015